RAPID COMMUNICATION

High-pressure synthesis, crystal structure, and electronic properties of $Ba_9Zr_{2.79}Te_{15}$

To cite this article: Runteng Chen *et al* 2026 *Chinese Phys. B* **35** 066101

RAPID COMMUNICATION

High-pressure synthesis, crystal structure, and electronic properties of $Ba_9Zr_{2.79}Te_{15}$

Runteng Chen(陈润滕)[1,2,†], Guodong Wang(王国东)[2,†], Zhe Wang(王哲)[3,†], Wenmin Li(李文敏)[4], Jianfa Zhao(赵建发)[2,5], Zheng Deng(邓正)[2,5], Heng Wang(王恒)[1,‡], Xiancheng Wang(望贤成)[2,5,§], Jun Zhang(张俊)[2,5,¶], and Changqing Jin(靳常青)[2,5,#]

[1] *College of Physics and Electronic Information Engineering, Guilin University of Technology, Guilin* 541008, *China*
[2] *Beijing National Laboratory for Condensed Matter Physics, Institute of Physics, Chinese Academy of Sciences, Beijing* 100190, *China*
[3] *College of Chemistry and Material Science, Hebei Normal University, Shijiazhuang* 050024, *China*
[4] *Institute of Quantum Materials and Physics, Henan Academy of Sciences, Zhengzhou* 450046, *China*
[5] *School of Physics, University of Chinese Academy of Sciences, Beijing* 100190, *China*

(Received 8 February 2026; revised manuscript received 13 March 2026; accepted manuscript online 16 March 2026)

The polycrystalline $Ba_9Zr_{2.79}Te_{15}$ sample was prepared by employing a solid-state synthesis method under high-temperature and high-pressure conditions. Comprehensive characterizations of structural and electrical properties were performed. $Ba_9Zr_{2.79}Te_{15}$ crystallizes in a hexagonal lattice with the space group $P\bar{6}c2$ (No. 188) and lattice parameters $a = 10.1977(8)$ Å and $c = 20.2646(9)$ Å. It is mainly composed of face-sharing $ZrTe_6$ octahedral chains extending along the *c*-axis, which form a triangular lattice in the *ab* plane. The Te chains are located in the middle of the $ZrTe_6$ triangular lattice. Electrical transport measurements indicate that $Ba_9Zr_{2.79}Te_{15}$ is a semiconductor. The thermal activation band gap of 0.23 eV is qualitatively discussed when compared with that of its sister compound $Ba_9Zr_3Se_{15}$, proving that the p electrons in the Te chains, with high quantum number orbitals, dominate electron conduction. Furthermore, the Debye temperature of $Ba_9Zr_{2.79}Te_{15}$ is calculated to be 157.28(9) K from thermodynamic measurements. The newly synthesized $Ba_9Zr_{2.79}Te_{15}$ with quasi-one-dimensional chain characteristics provides an opportunity for further exploration of diverse physical properties.

Keywords: high pressure synthesis, quasi one-dimensional structure, semiconductor

PACS: 61.05.cp, 61.66.Fn, 61.82.Fk, 65.40.Ba

DOI: 10.1088/1674-1056/ae521a **CSTR:** 32038.14.CPB.ae521a

1. Introduction

One-dimensional (1D) material systems have attracted considerable interest owing to their highly anisotropic crystal structures, which give rise to a range of novel physical phenomena, including superconductivity, electron spin/charge density waves (SDW/CDW), 1D–3D structure transition, and so on.[1,2] The structures along the 1D chains are also complex due to lattice distortion, which also has definite influences on the physical properties. Therefore, an emerging interest is to explore and synthesize 1D materials with new structures.

Among various 1D material systems, there are two types of typical 1D materials with the hexagonal Hf_5Sn_3Cu-anti-type structure. The RE_3MX_5 materials (RE = rare-earth metal, M = transition metal, X = P, As, Sb, and Bi)[3–14] can be assigned to the hexagonal space group ($P6_3/mcm$) and are characterized by 1D chains consisting of uniformly distributed face-sharing MX_6 octahedra. These materials exhibit diverse magnetic and metallic properties. Another typical material is the Ba_3MCh_5 family (M = transition metal, Ch = S, Se, Te).[15–29] This structure comprises infinitely extending face-sharing MCh_6 octahedral chains with different distortions and linear Ch chains along the *c*-axis, separated by Ba^{2+} ions with large interchain distances (typically > 9.5 Å), resulting in typical quasi-1D crystal structure and properties. In recent years, significant progress has been made in the Ba_3MCh_5 family, attributed to the diversity of structural distortions along the 1D chains. For example, $Ba_6Cr_2S_{10}$ stands out as a rare 1D ferrotoroidic candidate owing to the dimerized structure of CrS_6 chains,[21] while trimerized $Ba_9Fe_3Se_{15}$ undergoes a ferromagnetic-like phase transition at 14 K and a metallization transition at 29 GPa, accompanied by a spin-state crossover from high-spin to low-spin state.[23] Complex 1D structural features have been discovered in the Ba_3MSe_5 (M = Ti, Zr, Hf) system, such as tetramerization for Ti, trimerization for Zr, and uniform arrangement for Hf.[15]

[†] These authors contributed equally to this work.
[‡] Corresponding author. E-mail: wangh@glut.edu.cn
[§] Corresponding author. E-mail: wangxiancheng@iphy.ac.cn
[¶] Corresponding author. E-mail: zhang@iphy.ac.cn
[#] Corresponding author. E-mail: jin@iphy.ac.cn

In this work, we synthesized polycrystalline $Ba_9Zr_{2.79}Te_{15}$ for the first time. Its crystal structure, electrical transport properties, magnetic behavior, and thermodynamic characteristics have been systematically characterized and discussed.

2. Experimental details

Commercially available crystalline powders of Zr (Alfa, 99.5% pure), Te (Alfa, > 99.99% pure) and Ba lumps (Alfa, merged in oil, > 99.2% pure) were used as the starting materials. First, the BaTe precursor was synthesized by heating the mixture of Ba lumps and Te powder in an evacuated quartz tube at 700 °C for 33 hours. Subsequently, powders of BaTe, Zr and Te were homogeneously mixed according to a molar ratio of 3:1:2 and pressed into cylinders with a diameter of 6 mm and a height of 3 mm in an argon-filled glove box. A polycrystalline $Ba_9Zr_{2.79}Te_{15}$ sample was prepared via the solid-state synthesis method under high-temperature and high-pressure conditions using a 6×1400 T cubic anvil high-pressure apparatus. The pressure was gradually increased to 6 GPa, followed by heating to 1500 °C within 5 min. The temperature was held for 60 min and then quenched to room temperature before the pressure was released. Finally, pure black polycrystalline $Ba_9Zr_{2.79}Te_{15}$ samples were obtained.

Powder x-ray diffraction (XRD) measurements were conducted using a Rigaku Ultima IV (3 kW) diffractometer with Cu $K\alpha$ radiation ($\lambda = 1.5406$ Å, 40 kV, 40 mA). Data were collected over a 2θ range of 5°–125° with a step size of 0.02° per step. The Rietveld refinement was carried out using the GSAS and EXPGUI software packages.[30,31] The chemical composition of the samples was verified by energy-dispersive x-ray (EDX) spectroscopy (15 kV, 10 μA). Electrical transport properties were measured by a four-probe method with a measurement current of 10^{-6} A over a temperature range of 2–300 K using a physical property measurement system (PPMS). The specific heat measurement was carried out over a temperature range of 2–30 K. Magnetization measurements were performed using a superconducting quantum interference device (SQUID-VSM) under applied magnetic fields of 1000 Oe and 10000 Oe over the temperature range of 2–300 K.

3. Results and discussion

The powder XRD pattern of $Ba_9Zr_{2.79}Te_{15}$ synthesized under high-temperature and high-pressure conditions is presented in Fig. 1, which is indexed to a hexagonal structure by PowderX software[32] and is similar to that observed in quasi-1D $Ba_9Fe_3Se_{15}$.[23] Rietveld refinement was performed by adopting the structural model of $Ba_9Zr_3Se_{15}$,[15] which smoothly converged to $\chi^2 = 4.79(2)$, $R_{wp} = 8.12\%$ and $R_p = 5.52\%$. Refinement results show that $Ba_9Zr_{2.79}Te_{15}$ crystallizes in the hexagonal structure with the space group $P\bar{6}c2$ (No. 188). The lattice parameters are $a = b = 10.1977(8)$ Å, $c = 20.2646(9)$ Å, and the unit cell volume is 1825.08(2) Å^3. Detailed crystallographic data are summarized in Table 1.

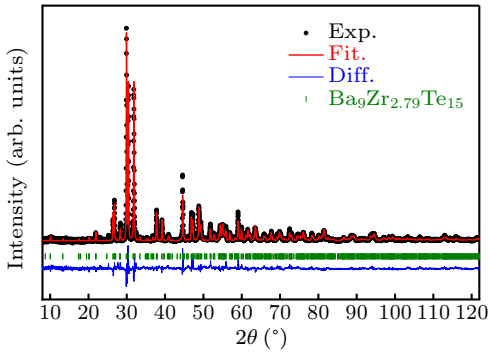

Fig. 1. The XRD pattern and the refinement spectra of $Ba_9Zr_{2.79}Te_{15}$.

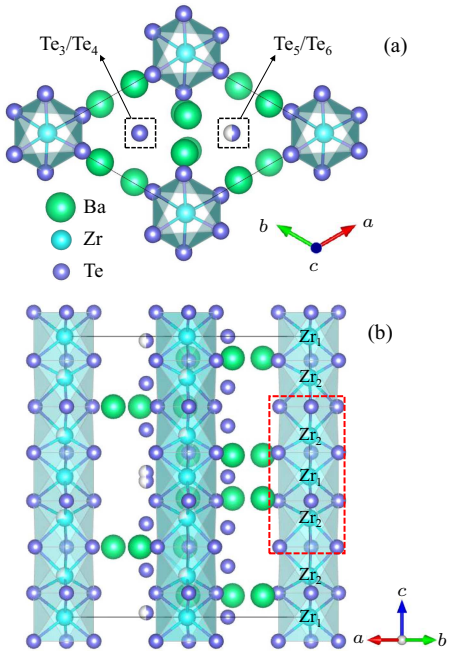

Fig. 2. Schematic crystal structure of the $Ba_9Zr_{2.79}Te_{15}$: (a) projection along the [001] direction; (b) projection along the [110] direction.

Based on the refinement results, the crystal structure schematic of $Ba_9Zr_{2.79}Te_{15}$ is presented in Fig. 2. Figures 2(a) and 2(b) show projections along the [001] and [110] directions, respectively, clearly illustrating the triangular lattice arrangement and linear chain geometry. The structure is mainly composed of face-sharing $ZrTe_6$ octahedral chains extending along the c-axis. These chains form a triangular lattice in the ab plane, where each Zr atom is located at the center of an octahedron surrounded by six Te atoms. The large interchain distance ($a > 10$ Å) confirms the typical 1D structural feature of $Ba_9Zr_{2.79}Te_{15}$. As shown in Fig. 3(a), there are two sites occupied by Zr atoms, Zr_1(0,0,0) and Zr_2(0,0,0.1465(3)), forming a Zr_2–Zr_1–Zr_2 trimer unit with adjacent Zr–Zr distances of 2.9693(9) Å and 4.1935(7) Å in the $ZrTe_6$ chains. The structural distortion can be reflected by the distances between Zr_1–Zr_2 and Zr_2–Zr_2 (see Table 1), which lead to three distinct Zr–Te bond lengths: Zr_2–Te_1 (2.7967(1) Å), Zr_1–Te_1

(3.0544(5) Å), and Zr_2–Te_2 (3.1761(4) Å). Herein, the degree of trimerization is defined as $(|d_{\text{inter}} - d_{\text{intra}}|)$: $(d_{\text{inter}} + d_{\text{intra}})$, where d_{inter} denotes the distance between adjacent Zr_2 atoms and d_{intra} the distance between adjacent Zr_1 and Zr_2 atoms in the 1D chains. Based on the bond length data presented in Table 1, the trimerization degree of $Ba_9Zr_{2.79}Te_{15}$ is calculated to be 17.1%. Furthermore, as shown in Fig. 3(b), additional Te atoms are situated at the middle of the triangular lattice to form two types of Te chains (Te_3–Te_4 and Te_5–Te_6), parallel to the 1D chains along the *c*-axis. The occupancy of Te_6 is 0.5. Within the Te chains, Te ions are arranged nonuniformly, with Te–Te distances varying from 2.7913(4) Å to 3.7017(1) Å. These bond lengths enable the formation of covalent bonds, similar to those found in $Ba_9Sn_3Te_{15}$.[29] Clearly, 2/3 of the Te atoms in the chains bond to each other forming $(Te_2)^{2-}$.

The coordination environment and bond lengths can affect the valence state of the central metal. The bond valence sum (BVS) model correlates the bond lengths around a metal center with its oxidation state. Using the following formula:

$$V_i = \sum \exp \frac{(R_0 - r_{ij})}{b},$$

where V_i is the valence state of atom i, r_{ij} is the bond length between atoms i and j, R_0 is the empirical bond distance parameter, and b is a universal constant of 0.37. For the Zr–Te bond, the R_0 is 2.67 Å. The oxidation states of Zr_1 and Zr_2 in $Ba_9Zr_{2.79}Te_{15}$ are estimated to be 2.1 and 2.9. That is, Zr_1 is +2 valence and Zr_2 is +3 valence.

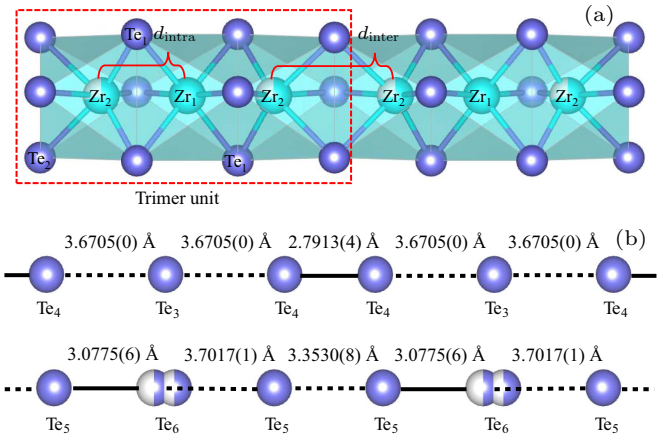

Fig. 3. Crystal structure details of $Ba_9Zr_{2.79}Te_{15}$: (a) $ZrTe_6$ octahedral chains; (b) Te chains.

Table 1. Crystallographic data of $Ba_9Zr_{2.79}Te_{15}$.

Formula:$Ba_9Zr_{2.79}Te_{15}$						
Crystal lattice			hexagonal			
Space group			$P\bar{6}c2$ (No.188)			
Lattice parameters (Å)			a = 10.1977(8) Å, c = 20.2646(9) Å			
Volume (Å^3)			1825.08(2)			
Formula weight (g/mol)			6745.53(3)			
Density (g/cm^3)			6.13(7)			
Refinement parameters			χ^2 = 4.79(2), R_{wp} = 8.12%, R_p = 5.52%			
Atomic parameters						
Atom	x	y	z	Occ.	U	Site
Ba_1	0.0079(8)	0.3797(5)	0.0768(9)	1	0.01(1)	12l
Ba_2	0.3973(1)	0.3825(3)	0.25	1	0.01(8)	6k
Zr_1	0	0	0	1	0.01(3)	2a
Zr_2	0	0	0.1465(3)	0.72(1)	0.04(0)	4g
Te_1	0.2387(5)	0.2531(5)	0.0858(0)	1	0.02(1)	12l
Te_2	0.0152(2)	0.2411(7)	0.25	1	0.01(2)	6k
Te_3	1/3	2/3	0	1	0.02(2)	2c
Te_4	1/3	2/3	0.1811(3)	1	0.00(6)	4h
Te_5	2/3	1/3	0.3327(3)	1	0.01(5)	4i
Te_6	2/3	1/3	0.0154(0)	0.5	0.03(6)	4i
Bond length (Å)						
Zr_1-Te_1	3.0544(5)		Zr_2-Te_2	3.1761(4)		
Zr_2-Te_1	2.7967(1)					
Te_4-Te_4	2.7913(4)		Te_5-Te_6	3.0775(6)/3.7017(1)		
The distance of adjacent atoms (Å)						
Zr_1-Zr_2	2.9693(9)		Zr_2-Zr_2	4.1935(7)		
Te_3-Te_4	3.6705(0)		Te_5-Te_5	3.3530(8)		
Valence state (from calculated results)						
Zr_1 = 2.1227(6)			Zr_2 = 2.8939(9)			
Occupation of Zr (from XRD refinement)						
Zr_1 = 1	Zr_2 = 0.72(1)		Average occupation of Zr: 0.81(4)			
Occupation of Zr (from EDX measurement) : 0.93(1)						

Scanning electron microscopy coupled with energy-dispersive x-ray spectroscopy (SEM–EDX) was used to analyze the elemental composition of the synthesized $Ba_9Zr_{2.79}Te_{15}$ samples. Five pieces of single crystal samples were chosen. The EDX results summarized in Table 2 confirm the presence of Ba, Zr, and Te, which are consistent with the starting materials. They yield an atomic ratio of Ba:Zr:Te = 3.00(0):0.93(1):4.89(7), which shows few defects in $Ba_9Zr_{2.79}Te_{15}$. Rietveld refinement of the XRD data reveals an average Zr occupancy of 81.4%. The discrepancy between the experimental and calculated results indicates the presence of Zr vacancies and the heterogeneity in the $Ba_9Zr_{2.79}Te_{15}$ sample. Considering covalently bonded Te atoms in the Te chains, the formal chemical formula can be expressed as $Ba_9Zr_{2.79}(Te^{2-})_9(Te_2^{2-}Te_4^{1-})$, which is consistent with the $Ba_9Sn_3Te_{15}$ system.[29]

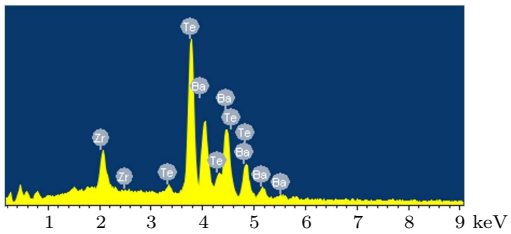

Fig. 4. Typical EDX spectroscopy for $Ba_9Zr_{2.79}Te_{15}$ sample.

Table 2. The chemical stoichiometry ratios of Ba, Zr and Te in the $Ba_9Zr_{2.79}Te_{15}$ sample.

Element	Weight percent (%)	Atomic percent (%)
Zr	7.58	10.55
Te	55.70	55.47
Ba	36.72	33.98
Total	100.00	100.00

Typically, structural distortions by forming superlattices can stabilize the crystal structure in 1D systems. Taking $Ba_9M_3Se_{15}$ (M = Ti, Zr and Hf) as an example, average tetramerization and trimerization distortions stabilize $Ba_{12}Ti_4Se_{20}$ and $Ba_9Zr_3Se_{15}$ structures, respectively, as the M metal ions change from the 3d to 4d period.[15] A trimerization degree of 17.1% leads to the formation of $Ba_9Zr_{2.79}Te_{15}$ in the present work. Meanwhile, Fermi surface nesting deriving from trimerization distortion usually exerts significant influence on the electronic transport properties of $Ba_9Zr_{2.79}Te_{15}$.[15] Following the structural analysis, the electrical transport properties of $Ba_9Zr_{2.79}Te_{15}$ were investigated using the four-probe method. Figure 5 shows the temperature dependence of the electrical resistivity. The resistivity increases as the temperature decreases, indicating typical semiconducting behavior. The inset in Fig. 5 shows the relationship between $\ln(R)$ and $1/T$, which exhibits a linear trend. The data were fitted using the thermal activation band gap formula

$$R \propto \exp\left(\frac{\Delta g}{2k_{\mathrm{B}}T}\right),$$

where Δg is the band gap and k_{B} is the Boltzmann constant, yielding a band gap of 0.23 eV. This demonstrates that the intrinsic conductivity in $Ba_9Zr_{2.79}Te_{15}$ is governed by a thermal activation mechanism. This resistive behavior agrees with the trimerization structure, which derives from Fermi surface nesting that induces the emergence of the band gap.

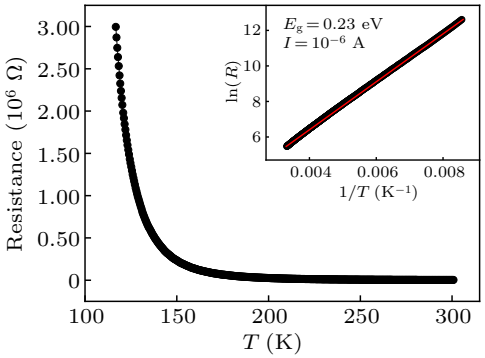

Fig. 5. Temperature dependence of the resistance of $Ba_9Zr_{2.79}Te_{15}$; the inset shows the relation of $\ln(R)$ versus $1/T$.

The magnetic properties of $Ba_9Zr_{2.79}Te_{15}$ were studied by measuring the temperature dependence of dc magnetization under an applied magnetic field of 1000 Oe over a temperature range of 2–300 K, using both zero-field cooling (ZFC) and field cooling (FC) modes. As shown in Fig. 6, the magnetization shows diamagnetism within the high temperature range and increases quickly as the temperature decreases, indicating paramagnetic behavior. The results were further confirmed by magnetization measurements under an applied magnetic field of 10000 Oe.

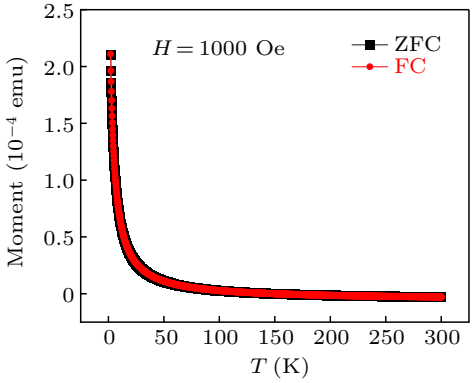

Fig. 6. Magnetic measurement results for the $Ba_9Zr_{2.79}Te_{15}$ sample.

Figure 7 presents the specific heat capacity data of $Ba_9Zr_{2.79}Te_{15}$. At low temperatures, the specific heat can be described by the formula $C/T = \gamma + \beta T^2$, where γ is the electronic contribution and βT^2 is the phonon contribution. The inset shows C/T as a function of T^2. The linear fitting yields a very small electronic specific heat coefficient γ, which is consistent with the semiconducting nature of the sample. The fitted β value is 13.48(7) mJ·mol^{-1}·K^{-4}. The Debye temperature was calculated using the formula

$$C_V = \frac{12}{5}\pi^4 N k_{\mathrm{B}} \frac{T^3}{\Theta_{\mathrm{D}}^3},$$

where $N = n \times N_A$ (n is the number of atoms per formula unit; N_A is Avogadro's constant), k_B is the Boltzmann constant, and Θ_D is the Debye temperature. The calculated Debye temperature of $Ba_9Zr_{2.79}Te_{15}$ is 157.28(9) K.

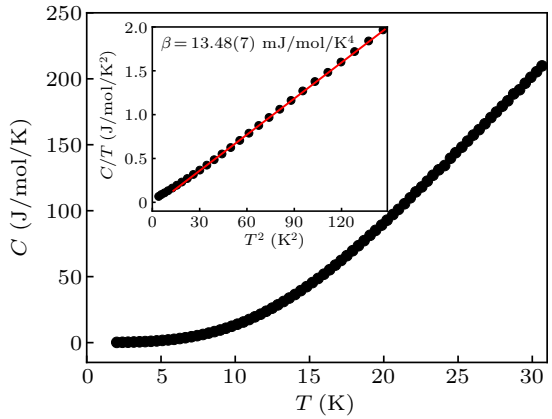

Fig. 7. Specific heat capacity data of $Ba_9Zr_{2.79}Te_{15}$; the inset shows the relation of C/T versus T^2.

To better understand the electronic transport mechanism of $Ba_9Zr_{2.79}Te_{15}$, we compared the thermal activation band gap with that of its sister compound $Ba_9Zr_3Se_{15}$. The band gap of $Ba_9Zr_{2.79}Te_{15}$ is 0.23 eV, which is significantly narrower than the 1.20 eV in $Ba_9Zr_3Se_{15}$.[15] This obvious difference stems from the inherent electronic structure characteristics of Te and Se atoms. In comparison with Se, Te atoms are characterized by p orbitals with a higher quantum number, which allows them to extend further in space and gives rise to weaker localization. In $Ba_9Zr_{2.79}Te_{15}$, the p electrons in the Te chains with high quantum number orbitals enhance interchain orbital overlap, facilitating easier electron hopping between the interchains. Moreover, the electronegativity of Te is lower than that of Se, which further promotes the delocalization of charge carriers. Notably, the Zr vacancies present in $Ba_9Zr_{2.79}Te_{15}$ also exert a certain effect on the electronic structure, as the disorder induced by vacancies tends to localize electrons in $ZrTe_6$ chains and is unfavorable to electron hopping. Therefore, the p electrons in the Te chains mainly contribute to the electrical transport behavior in $Ba_9Zr_{2.79}Te_{15}$.

4. Conclusion

We successfully synthesized the quasi-1D hexagonal compound $Ba_9Zr_{2.79}Te_{15}$ for the first time using a high-temperature and high-pressure method. Structural analysis reveals that $Ba_9Zr_{2.79}Te_{15}$ is composed of trimerized $ZrTe_6$ octahedral chains and linear Te chains separated by Ba^{2+} ions. Electrical transport and thermodynamic measurements demonstrate that $Ba_9Zr_{2.79}Te_{15}$ is a semiconductor with a band gap of 0.23 eV, in which electronic hopping is dominated by the p electrons in the Te chains. This study enriches the Ba_3MCh_5 material family and provides a new platform for investigating physical properties.

Acknowledgements

Project supported by the National Key R&D Program of China (Grant Nos. 2023YFA1406001 and 2024YFA140800) and the National Natural Science Foundation of China (Grant Nos. 12104488 and 12474097).

References

[1] Petrović A P, Ansermet D, Chernyshov D, Hoesch M, Salloum D, Gougeon P, Potel M, Boeri L and Panagopoulos C 2016 *Nat. Commun.* **7** 12262
[2] dos Santos C A M, White B D, Yu Y K, Neumeier J J and Souza J A 2007 *Phys. Rev. Lett.* **98** 266405
[3] Xu Z C, Wang Y X, Zhang C W, Liu H X, Han X, Wu L S, Zhang X M, Wu Q S and Shi Y G 2024 *Phys. Rev. B* **110** 165106
[4] Duan L, Zhang J, Wang X C, Zhao J F, Cao L P, Li W M, Deng Z, Yu R Z, Li Z and Jin C Q 2020 *J. Alloys Compd.* **831** 154697
[5] Fu L C, Shi L C, Chen X M, Duan L, Peng Y, Zhang J, Song J, Deng Z, Zhang S J, Zhao J F, Liu Y, Zhang J F, Zhu J L, Wang X C and Jin C Q 2024 *J. Phys.: Condens. Matter* **37** 015803
[6] Bolloré G, Ferguson M J, Hushagen R W and Mar A 1995 *Chem. Mater.* **7** 2229
[7] Moore S H D, Deakin L, Ferguson M J and Mar A 2002 *Chem. Mater.* **14** 4867
[8] Matin M, Kulkarni R, Thamizhavel A, Dhar S K, Provino A and Manfrinetti P 2017 *J. Phys.: Condens. Matter* **29** 145601
[9] Murakami T, Yamamoto T, Takeiri F, Nakano K and Kageyama H 2017 *Inorg. Chem.* **56** 5041
[10] Gauthier N, Sibille R, Pomjakushin V, Fjellvåg Ø S, Fraser J, Desmarais M, Bianchi A D and Quilliam J A 2024 *Phys. Rev. B* **109** L140405
[11] Ferguson M J, Hushagen R W and Mar A 1997 *J. Alloys Compd.* **249** 191
[12] Duan L, Wang X C, Zhan F Y, Zhang J, Hu Z W, Zhao J F, Li W M, Cao L P, Deng Z, Yu R Z, Lin H J, Chen C, Wang R and Jin C Q 2020 *Science China Materials* **63** 1750
[13] Duan L, Wang X C, Zhang J, Zhao J F, Zhao Z W, Xiao C J, Guan C L, Wang S, Shi L P, Zhu J L and Jin C Q 2022 *J. Alloys Compd.* **905** 164214
[14] Duan L, Wang X C, Zhang J, Hu Z, Zhao J F, Feng Y G, Zhang H L, Lin H J, Chen C T, Wu W, Li Z, Wang R, Zhang J F, Xiang T and Jin C Q 2022 *Phys. Rev. B* **106** 184405
[15] Wang Z L, Wang G D, Li W M, Wang Z, Chen R T, Duan L, Zhao J F, Deng Z, Zhang J F, Yan T J, Zhang J, Wang X C and Jin C Q 2025 *Inorg. Chem.* **64** 13705
[16] Zhang J, Jia Y T, Wang X C, Li Z, Duan L, Li W M, Zhao J F, Cao L P, Dai G Y, Deng Z, Zhang S J, Feng S M, Yu R Z, Liu Q Q, Hu J P, Zhu J L and Jin C Q 2019 *NPG Asia Mater.* **11** 60
[17] Wang Z L, Wang G D, Li W M, Chen R T, Duan L, Zhao J F, Deng Z, Zhang J F, Yan T J, Zhang J, Wang X C and Jin C Q 2025 *Chin. Phys. B* **34** 086101
[18] Almoussawi B, Tomohiri H, Kageyama H and Kabbour H 2021 *Eur. J. Inorg. Chem.* **2021** 1271
[19] Zhang J, Liu M, Wang X C, Zhao K, Duan L, Li W M, Zhao J F, Cao L P, Dai G Y, Deng Z, Feng S M, Zhang S J, Liu Q Q, Yang Y F and Jin C Q 2018 *J. Phys.: Condens. Matter* **30** 214001
[20] Zhang J, Zhang X Y, Xia Y H, Zhao J F, Duan L, Wang G D, Min B S, Cao H B, Dela Cruz C R, Zhao K, Sun H Y, Zhu J L, Zhang J F, Xiang T, Wang X C and Jin C Q 2023 *Phys. Rev. B* **108** 174423
[21] Zhang J, Wang X C, Zhou L, Liu G X, Adroja D T, da Silva I, Demmel F, Khalyavin D, Sannigrahi J, Nair H S, Duan L, Zhao J F, Deng Z, Yu R Z, Shen X, Yu R C, Zhao H, Zhao J M, Long Y W, Hu Z W, Lin H J, Chan T S, Chen C T, Wu W and Jin C Q 2022 *Adv. Mater.* **34** 2106728
[22] Zhang J, Jia Y T, Chen X M, Min B S, Honda T, Hu Z W, Tjeng L H, Shamoto S I, Zhao J F, Deng Z, Song J, Duan L, Valvidares M, Zhu J L, Wang X C and Jin C Q 2025 *Phys. Rev. B* **111** 224405
[23] Zhang J, Komarek A C, Jin M L, Wang X C, Jia Y T, Zhao J F, Li W M, Hu Z W, Peng W, Wang X, Tjeng L H, Deng Z, Yu R Z, Feng S M, Zhang S J, Liu M, Yang Y F, Lin H J, Chen C T, Li X D, Zhu J L and Jin C Q 2021 *Phys. Rev. Mater.* **5** 054606

[24] Zhang J, Jin M L, Li X, Wang X C, Zhao J F, Liu Y, Duan L, Li W M, Cao L P, Chen B J, Wang L J, Sun F, Wang Y G, Yang L X, Xiao Y M, Deng Z, Feng S M, Jin C Q and Zhu J L 2020 *Chin. Phys. Lett.* **37** 087106

[25] Zhang J, Duan L, Wang Z, Wang X C, Zhao J F, Jin M L, Li W M, Zhang C L, Cao L P, Deng Z, Hu Z W, Agrestini S, Valvidares M, Lin H J, Chen C T, Zhu J L and Jin C Q 2020 *Inorg. Chem.* **59** 5377

[26] Duan L, Wang X C, Zhang J, Zhao J F, Li W M, Cao L P, Zhao Z W, Xiao C J, Ren Y, Wang S, Zhu J L and Jin C Q 2021 *Chin. Phys. B* **30** 106101

[27] Duan L, Wang X C, Zhang J, Zhao J F, Cao L P, Li W M, Yu R Z, Deng Z and Jin C Q 2020 *Chin. Phys. B* **29** 036102

[28] Duan L, Chen X M, Wang Z L, Wei Y T, Zhang J, Feng Y G, Wang S, Du S X, Zhao Z W, Xiao C J, Wang X C and Jin C Q 2024 *J. Alloys Compd.* **1007** 176496

[29] Zhang J, Su R, Wang X C, Li W M, Zhao J F, Deng Z, Zhang S J, Feng S M, Liu Q Q, Zhao H Z, Guan P F and Jin C Q 2017 *Inorg. Chem. Front.* **4** 1337

[30] Toby B H 2001 *J. Appl. Crystallogr.* **34** 210

[31] Larson A C and Von Dreele R B 2004 *Los Alamos National Laboratory Report LAUR* 86

[32] Dong C 1999 *J. Appl. Crystallogr.* **32** 838